Tasmania Department Of Mines — Report 1992/34

Contact metamorphism of the Mathinna Beds and the depth of crustal residence during mega-kinking in northeast Tasmania

by B. D. Goscombe, M. P. McClenaghan and J. L. Everard

Abstract

After tight folding and formation of a steep penetrative cleavage, the Mathinna Beds of northeast Tasmania were intruded by numerous large granite-granodiorite batholiths at 356–398 Ma. These intrusions contact metamorphosed the Mathinna Beds, giving rise to the spotted metapelites with cordierite-muscovite-biotite-quartz-K feldspar-ilmenite-rutile ± andalusite ± plagioclase assemblages. Geothermobarometry, equilibrium thermodynamics, and the experimental and theoretically defined stability field of the above assemblage, define contact metamorphic conditions to have been >450–500°C and 1000–1750 bar. Geothermometry of the Upper Blessington granodiorite and the samples from the Scottsdale Batholith indicate the temperature of these melts during intrusion to be 650–700°C. Both this estimate of the crytallisation temperature and the T_{max} experienced by the thermal aureole suggest that the Scottsdale Batholith was intruded as a relatively cool granitoid. This is confirmed by the narrow contact aureole and absence of partial melting of the host Mathinna Beds. The relatively cool intrusion temperature suggests that the melt was derived from much deeper crustal levels, and was possibly emplaced as a partially crystallised body into the upper crust.

An additional factor to be considered is the large temperature gradient (200°C) between the granitoid and the contact aureole. This suggests the absence of the thermal insulation effect of a thick section of overlying crust. Absence of this thermal "blanketing" resulted in a short-lived thermal pulse in the contact aureole, with very little thermal energy being imparted into the contact metamorphosed rocks.

Geobarometry estimates from the Scottsdale Batholith samples indicate emplacement of this body at 900–1300 bar (3.15–4.55 km depth). Such an extremely shallow depth of emplacement is consistent with pressure estimates from the thermal aureole, and is confirmed by the close proximity of coeval rhyolitic extrusive rocks of the St Marys Porphyrite. Such a shallow level of intrusion further supports the absence of an insulating layer of overlying crust to be also responsible for the low temperatures experienced by the thermal aureole.

Kinking of the Mathinna Beds occurred on all scales throughout northeast Tasmania after granitoid emplacement and before deposition of the Parmeener Supergroup at approximately 210–300 Ma. The extremely shallow crustal level, of the rocks presently exposed, at the time of granitoid emplacement is consistent with the nature of the mega-kinking style of deformation. The brittle and instantaneous nature of this kinking event is entirely consistent with the style of tectonics expected in the brittle zone of the shallow upper crust.

INTRODUCTION

The structural events experienced in northeast Tasmania have been reasonably well documented with respect to the styles of deformations and their respective stress fields (Williams, 1970; Goscombe and Findlay, 1989). Such information forms the backbone for elucidating tectonic histories and models for the region. However, structural based tectonic models may be too loosely constrained if there is no knowledge of the depth of crustal residence during deformation. This report confidently constrains the depth of crustal residence, of rocks presently exposed at the surface, during emplacement of the Devonian granitoid batholiths of northeast Tasmania.

In the absence of any crustal over-thickening event between granitoid emplacement and the mega-kinking of northeast Tasmania, mega-kinking is assumed to have occurred at the same crustal level as the emplacement of the presently exposed granitoids. This estimate of the depth of burial during the mega-kinking event adds a more comprehensive outline of the crustal conditions during this tectonic event, and possibly for mega-kinking style tectonics in general.

The thermal as well as the barometric conditions associated with emplacement of the Scottsdale Batholith are constrained, both for the granitoid and its contact metamorphic aureole. Petrology and mineral chemistry of the contact aureole spotted metapelites are presented in detail. These data are utilised in constraining the P and T conditions of formation by employing:

- geothermobarometry (using nine different mineral equilibria);
- equilibrium thermodynamics (Powell and Holland, 1988);

- experimental and theoretical stability fields of relevant mineral parageneses.

Samples 373 to 392 were collected and analysed by B. Goscombe during mapping of the Alberton Quadrangle in 1989–92 (fig. 1). Samples BJ62D and BJ642A were collected and analysed by J. Everard, and the Scottsdale Batholith samples (prefixed by SB) were collected and analysed by M. P. McClenaghan during mapping of the Alberton Quadrangle.

REGIONAL GEOLOGY

The rocks of northeast Tasmania consist of a turbiditic sequence of alternating sandstone and siltstone-mudstone of Early Ordovician (Banks and Smith, 1968) and Early Devonian (Rickards and Banks, 1979) age. These were very tightly folded (D_1) at some stage prior to emplacement of Late Devonian granitoids. D_1 folding produced a pervasive penetrative cleavage of aligned fine-grained phyllosilicates of very low metamorphic grade (sub-greenschist, <<300°C). For most of northeast Tasmania this cleavage is near vertical and trends approximately N-S to NW-SE (fig. 1). This deformational period may have had a complex history as suggested by the presence of transgressed folds and episodic fold tightening (Williams, 1970). However, an overall E-W to NE-SW directed crustal shortening was experienced.

In the Late Devonian (356–398 Ma; Cocker, 1982) numerous granite-granodiorite batholiths were intruded and at the same time the St Marys porphyrite was extruded. Thin (typically 1–2 km wide in map section) contact metamorphic aureoles were developed around these batholiths. These aureoles are mapped as the limit of spotting in the pelitic units of the Mathinna Beds. These spots are ameboid-rounded poikiloblastic clots of cordierite up to 5 mm in diameter. Gravity data suggest that only the upper portions of these batholiths are presently exposed and the batholith margin dips relatively shallowly outwards.

No mineral zones or isograds are developed within the contact aureoles. The same assemblage of cordierite-muscovite-biotite-quartz-K feldspar-ilmenite ± rutile ± andalusite ± plagioclase (Table 1) is developed throughout the whole recognisable aureole of spotted metapelite. Beyond this aureole are typical low-grade pelites with no thermal effect visible in hand specimen and thin section.

At some time subsequent to pluton emplacement the whole of northeast Tasmania was subject to N-S directed horizontal compressive stress (D_2). This resulted in monoclinic kinkbands with sharp angular hinges being developed on centimetre, metre and kilometre scales (fig 1.). D_2 deformation was of a brittle nature with sharp discontinuities in hinges accompanied by fracturing and "ripping" of phyllosilicate mineral grains. These kinkband structures possibly formed on a nearly instantaneous (in a geological sense) time frame. There was no thickening of the vertical crustal pile during kinking as all N-S crustal shortening was accommodated by E-W directed crustal extension (i.e. the kink fold axes are vertical). No structural expressions of D_2 N-S shortening have been identified from within the granitoid batholiths. D_2 strain was partitioned into the Mathinna Beds in preference to the more competent and large homogeneous batholiths. No volume problems in accommodating this heterogeneous strain distribution are anticipated because D_2 bulk shortening was very small (3–8%; Goscombe and Findlay, 1989). Small-scale kinkbands overprint the cordierite-biotite-muscovite contact aureole assemblage by sharply kinking the micas and bending elongate cordierite poikiloblasts.

Subsequent to kinking and granitoid intrusion, the northeast of Tasmania was denuded approximately to the crustal level that is presently exposed. The Parmeener Supergroup was deposited on this unconformity during the period 300–210 Ma. During Tertiary and Recent times northeast Tasmania was uplifted with accompanying normal faulting and was eroded to crustal levels equivalent to, and slightly deeper than, the crustal level exposed prior to deposition of the Parmeener Supergroup.

PETROLOGY OF THE SPOTTED METAPELITES

Only the metapelitic samples of contact metamorphosed Mathinna Beds are of metamorphic interest in this report. The meta-psammitic samples are polygonal granoblastic quartzites with scattered but aligned fine-grained muscovite, biotite and opaque grains. Spotted metapelites were collected in a traverse of 1200 m length at a high angle to the Scottsdale Batholith contact (fig. 1). These samples all consist of a fine to medium-grained polygonal granoblastic quartz-rich matrix with minor K-feldspar, and are mica-rich and highly foliated. The muscovite and biotite laths are in textural equilibrium with the quartz and K-feldspar and are aligned parallel to the S_1 fold axial planar cleavage. Micas are typically stubby and not highly elongate and a large proportion are not aligned with the S_1 cleavage. Biotite is always a primary matrix phase and muscovite is mostly likewise, but muscovite also occurs as a retrograde phase replacing cordierite.

Cordierite occurs as 0.5–5 mm ameboid poikiloblastic blobs and distinct ellipsoid poikiloblasts. These often form a seive texture because of the high density of quartz (mostly), biotite and muscovite inclusions. Some cordierite poikiloblasts are ellipsoid in shape and have pressure shadows consisting of higher concentrations of micas. This flattening may be associated with stresses due to granite emplacement. Cordierite is commonly totally retrogressed to chlorite and white mica mixtures. When very fine grained this appears to be the one pale green mineral phase; such mixtures are called pinnite. All chlorite is retrograde. None has been identified in textural equilibrium with cordierite or muscovite and biotite in the matrix. Andalusite has only been identified in two samples as medium-grained irregular-shaped inclusions within cordierite. All opaque minerals are ilmenite-rich ilmenite-hematite solid solution with minor amounts of intergrown rutile.

Elongate cordierites are bent by centimetre-scale kinkbands. These bend, kink and fracture biotite and muscovite laths, and no new mineral grains nor overgrowths are crystallised within the hinges and fold axial planes of the kinkbands. Thus kinking must have

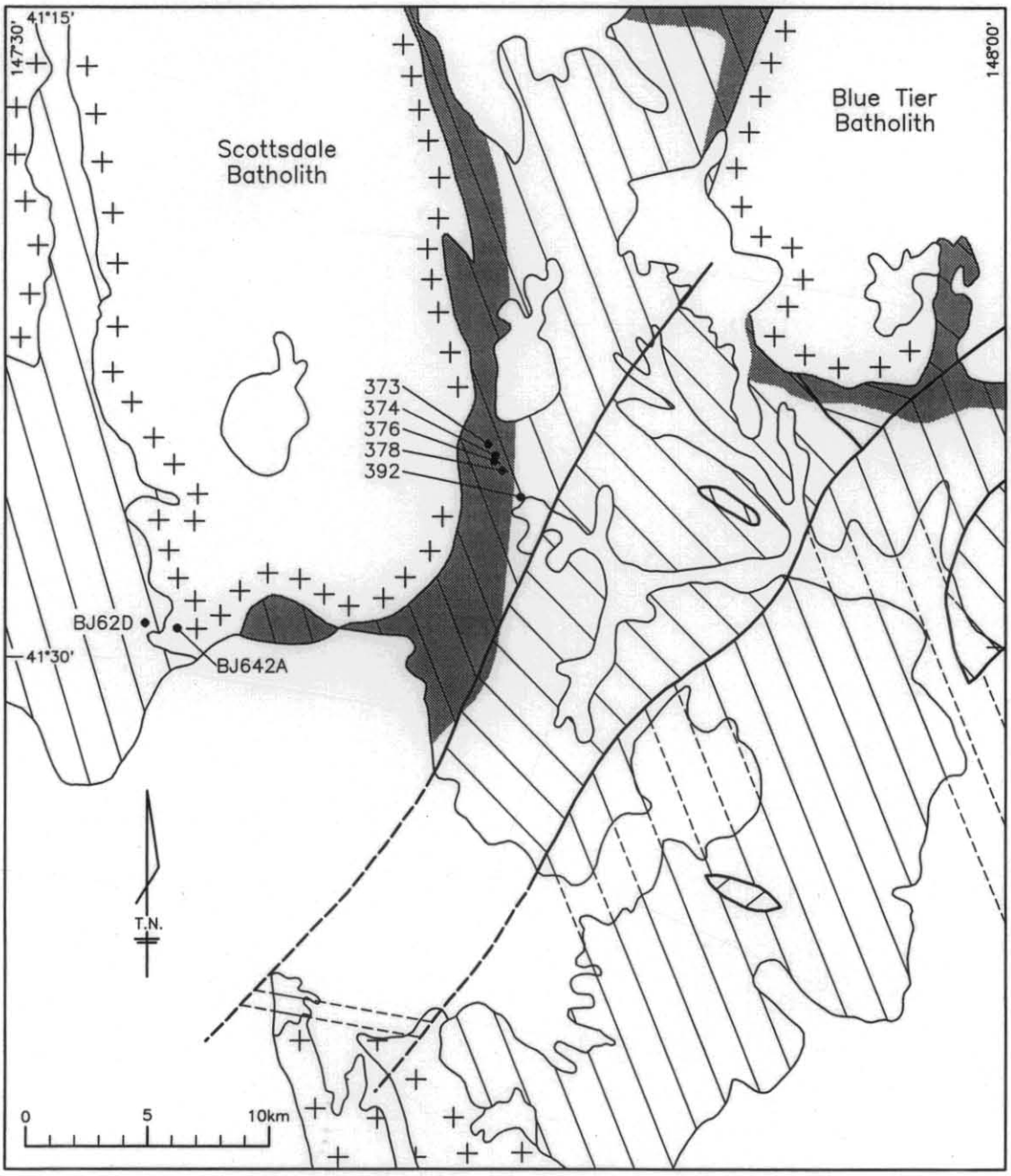

Mathinna Beds: D_1 cleavage trace and D_2 megakink axial trace.

Devonian granitoids.

Contact aureole where recognised by spotting.

Parmeener Supergroup and younger cover.

Figure 1

Simplified geological map of Northeast Tasmania, outlining major Devonian Batholiths, limit of associated contact aureole cordierite development (spotted pelites), D_1 structural trends (the penetrative fold axial planar cleavage), D_2 mega-kinks, and locations of the samples used in this report. Samples prefixed by SB are from locations within the Scottsdale Batholith.

5 cm

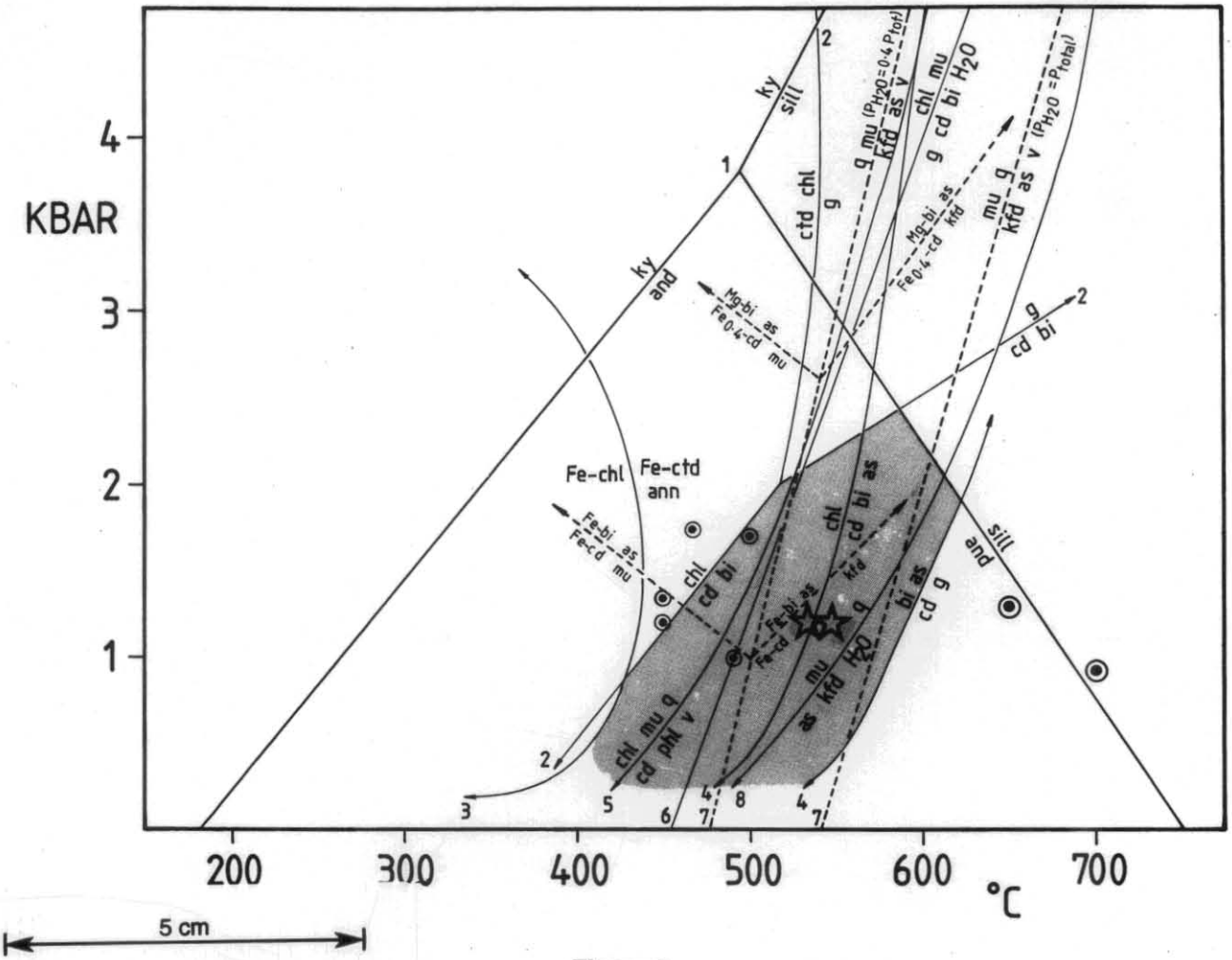

Figure 2

Collation of published experimental and theoretically calculated phase equilibria for pelitic systems. Shaded region is the stability field of spotted pelite assemblages from rocks adjacent to the Scottsdale Batholith. Small circles with dots are the preferred P-T loci (Table 10) of the five spotted pelite samples (BJ62D, 373C, 373J, 373N and 374). Stars are the P-T loci of samples (BJ62D and 373J) constrained by temperatures estimated by equilibrium thermodynamics and pressures assumed to be 1.2 kbar. Large circles with dots are the preferred P-T loci (Table 10) of the Scottsdale Batholith samples (BJ642A and an average of all SB samples).

(1) Aluminosilicate stability (Spear and Cheney, 1989).

(2) Theoretically calculated equilibria in KFASH (Powell and Holland, 1990).

(3) Theoretically calculated equilibria in KFASH (Spear and Cheney, 1989).

(4) Theoretically calculated equilibria in KFMASH (Spear and Cheney, 1989).

(5) Experimentally derived equilibria in KMASH (Massone, 1989).

(6) Experimentally derived equilibria in KFMASH (Burnell and Rutherford, 1984).

(7) Experimentally derived equilibria in KFMASH for different water pressure (Holdaway and Lee, 1977).

(8) Experimentally derived muscovite breakdown (Evans, 1965; see Hesen and Green, 1973).

occurred at some stage after granitoid intrusion and the waning of the thermal pulse.

The ubiquitous contact aureole assemblage; cd-mu-bi-q ± kfd ± and, forms in a relatively tightly constrained P-T window when compared to published experimental and theoretical phase relationships for pelites (fig. 2). The lower temperature limit of this assemblage (400–500°C) is defined by reactions involving chlorite ± muscovite breaking down to cordierite-biotite in the K_2O-FeO-Al_2O_3-SiO_2-H_2O (KFASH) system (Spear and Cheney, 1989; Powell and Holland, 1990; Burnell and Rutherford, 1984) and the K_2O-MgO-Al_2O_3-SiO_2-H_2O (KMASH) system (Massone, 1989). The upper temperature limit (550–600°C) is constrained by muscovite breakdown reactions. The upper pressure limit (2400 bar) is defined by the andalusite stability field and the breakdown of cordierite-biotite to garnet assemblages in KFASH (Powell and Holland, 1990) (fig. 2).

MINERAL CHEMISTRY

All mineral samples, except BJ62D and those from the Scottsdale Batholith (BJ642A and all those prefixed by SB), were analysed using the Cameca SX50 electron microprobe in the Central Science Laboratory at the University of Tasmania by B. Goscombe. Analysing conditions were by wavelength dispersive mode with an accelerating voltage of 20 kV and beam current of 20 nA (10 nA for micas) with magnification of 20,000 (10,000 for micas). Samples BJ62D and BJ642A and Scottsdale Batholith samples (prefixed by SB) were analysed by J. Everard and M. McClenaghan repectively. These were analysed using the JEOL JXA50A electron microprobe at the University of Tasmania with operating conditions of 15kV and 0.7 nA in energy dispersive mode. All mineral analyses have been recalculated for cation proportions using the program RECALC (Powell and Holland, 1988). Only selected representative analyses are contained in Appendix 1; a complete set of the mineral analyses used in this report can be obtained from B. Goscombe. Although mineral analyses from the Scottsdale Batholith have been used for geothermo-barometry, they are not described in this report. Representative analyses are presented in the appendix.

Cordierite in all samples has Fe/(Fe+Mg) ratios ranging from 43 to 51% and averaging 46% (sample BJ62D is 35.5%). These are relatively Fe-rich compared to samples in the literature from both regional metamorphic (5–25%) and contact metamorphic and sanidinite facies (14–53%) environments (Deer *et al.*, 1966; Schreyer *et al.*, 1990). There is no significant departure of the Al/Si ratio from the ideal 4:5. TiO_2 is absent in most analyses with a maximum of 0.08%. K_2O, CaO and MnO are all insignificantly low, averaging 0.04%, 0.03% and 0.09% respectively. Na_2O is consistently $0.20 \pm 0.02\%$. Fe_2O_3 contents vary widely, ranging from 0.12 to 1.79%. Analysis totals are all relatively high for cordierites (>98%), suggesting a low CO_2-H_2O volatile component in the structure. This is normal for cordierites formed at low pressures (Vry *et al.*, 1990; Schreyer *et al.*, 1990; Miyake 1990). There is no correlation between distance of the sample from the Scottsdale Batholith and the Fe-Mg distribution coefficient between coexisting biotite and cordierite (Appendix 2).

Muscovite Fe/Fe+Mg ratios range from 22 to 33% and average 27%, except sample BJ62D which averages 52%. All muscovites were recalculated assuming 60% of all Fe is Fe^{3+}. The paragonite component in all samples was low, Na/(Na+K) ranging from 7.0 to 10.3% (average 8.23%). MnO and CaO are absent or insignificantly low. TiO_2 contents range from 0.00 to 1.17% (average 0.70%). Si cation contents, based on 12 oxygen, are very low and range from 2.97 to 3.16% (average 3.07, for 23 analyses).

Biotite Fe/(Fe+Mg) ratios range from 48.5 to 60.5% and average 54.5%, thus they are biotites, not phlogopite (Deer *et al.*, 1974). All biotites have been recalculated assuming 15% of the Fe is Fe^{3+}. The Si/(Si+Al) ratios range from 53.2 to 61.3% and average 59.0% and so these biotites have a very high siderophyllite component. TiO_2 contents are relatively low, ranging from 0.12 to 3.29% (average 2.19%). Na_2O, CaO and MnO are insignificantly low, ranging 0.05–0.98%, 0.00–0.16% and 0.0–0.23% respectively.

Feldspars are dominated by K-Feldspar; these have compositions ranging from 76–89% orthoclase with insignificant anorthoclase. No exsolution lamelli have been observed in these feldspars. Albitic plagioclase (ab = 85%, an = 14%, or = 0.7%) occurs in sample BJ62D. The andalusite in sample 373N is very pure, with 0.26% FeO being the only impurity.

The only Fe-Ti oxides recognised are isolated fine grains of ilmenite-hematite solid solution and rutile. Ilmenite and rutile are also finely intergrown on a sub-microscopic scale. Ilmenite-hematite solid solution ranges in composition from ilm = 100–98%, hem = 0–2%. Ilmenite-rutile intergrowths range in composition from rut = 91–66%, ilm = 9–34%. The very low hematite contents and common presence of rutile (Table 1) suggests low O_2-fugacity (reducing) conditions.

Chlorite Fe/(Fe+Mg) ratios average 49.3% and Si cations (for 28 oxygen) average 5.33%, thus these are ripidolite chlorites (Deer *et al.*, 1966).

GEOTHERMOMETRY

The biotite-muscovite Fe-Mg exchange (Hoisch, 1989), two feldspar (Powell and Powell, 1977), biotite-chlorite Fe-Mg exchange (Laird, 1989) and Al in chlorite (Cathelineau, 1988) geothermometers have been applied to the spotted metapelites. The results are tabulated in Tables 2–4 and plotted in Figures 3 and 4. For a pressure estimate of 1kbar the average biotite-muscovite temperature is 437°C and the average two feldspar temperature is 456°C. These results are not only consistent with each other but are consistent with, but slightly lower than, the temperature range of the phase stability field for spotted metapelite assemblages (fig. 2). The slightly lower biotite-muscovite temperatures with respect to the phase stability constraints may reflect either the geothermometer calibration or possibly re-equilibration of the mineral pairs during cooling after T_{max}.

There is no consistent gradient in temperature from the samples closest to the Scottsdale Batholith and those most distant (Table 1 and 2). The chlorite and biotite-chlorite geothermometers cannot be considered reliable for estimating peak thermal conditions because chlorite is, in most samples, a retrogressive mineral replacing peak-metamorphic cordierite. The late-stage retrogressive nature of chlorite is reflected by the low temperatures resulting from these two geothermometers. The disequilibrium between peak metamorphic biotite and retrograde chlorite is reflected by the inconsistent set of results from the one sample (373C) (Table 4).

The temperature of crystallisation of the Scottsdale Batholith (granodiorites) is estimated using the two feldspar (Powell and Powell, 1977), hornblende-plagioclase (Blundy and Holland, 1990) and biotite-clinopyroxene and hornblende-clinopyroxene (Perchuk *et al.*, 1985) geothermometers (Table 5, fig. 4). For a pressure estimate of 1.2 kbar the average results are 698°C, 683°C and 668°C for the hn-pl, bi-cpx and hn-cpx pairs respectively. These results are very consistent with each other and so are considered real estimates of the temperature of crystallisation of the Scottsdale Batholith. The temperature of granite crystallisation is presumably

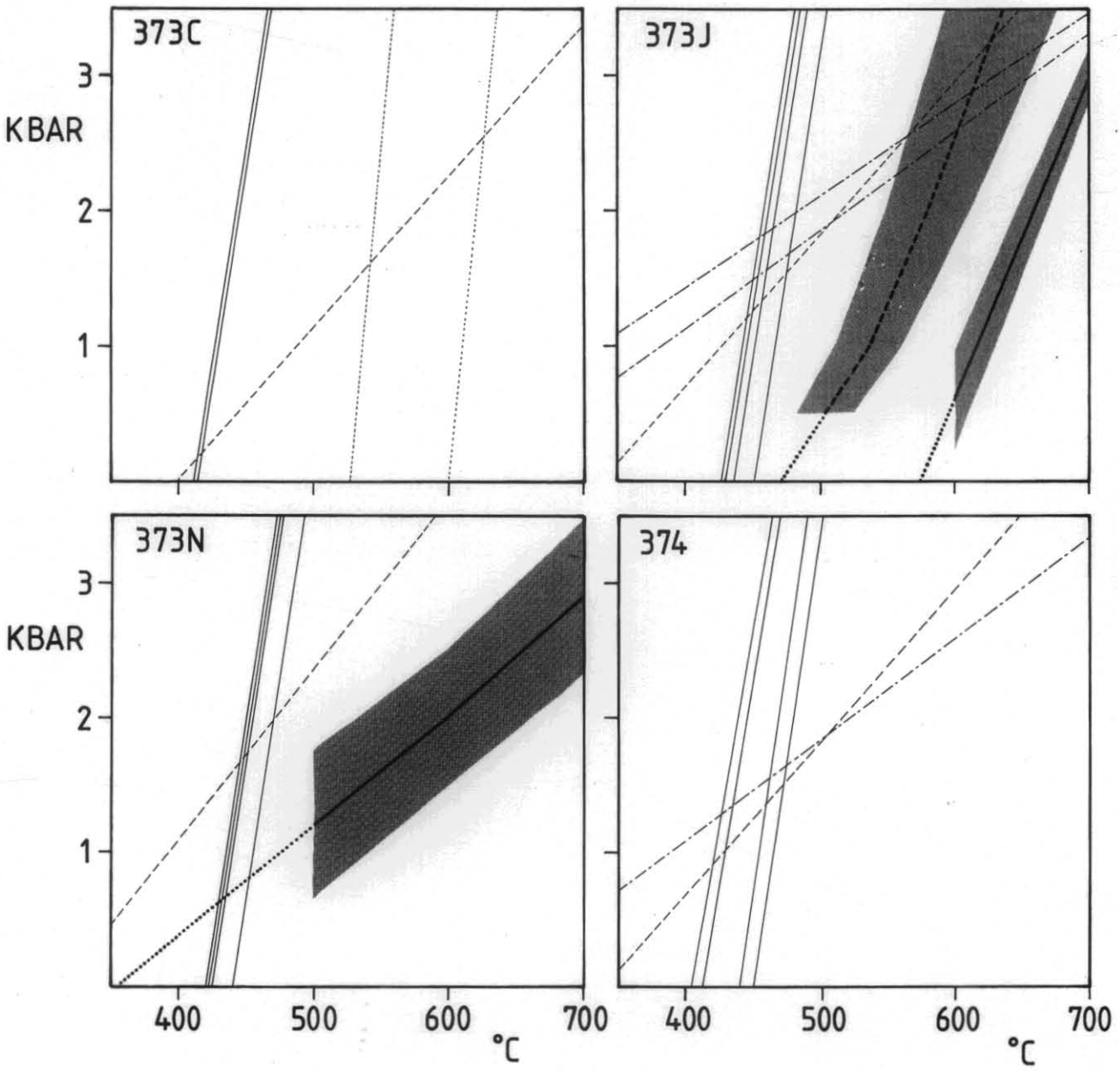

Figure 3

Plots of geothermometer, geobarometer and equilibrium thermodynamics calculations for the four spotted pelite samples (373C, 373J, 373N & 374).

solid thick line	—	Average P by equilibrium thermodynamics
dashed thick line	—	Average T by equilibrium thermodynamics
shaded region	—	Errors for equilibrium thermodynamics
solid thin line	—	Biotite-muscovite geothermometry
dotted thin line	—	Biotite-chlorite geothermometry
dashed line	—	Phengite geobarometry
dot-dashed line	—	Biotite–muscovite–K-feldspar geobarometry.

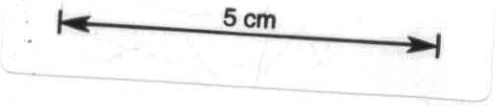

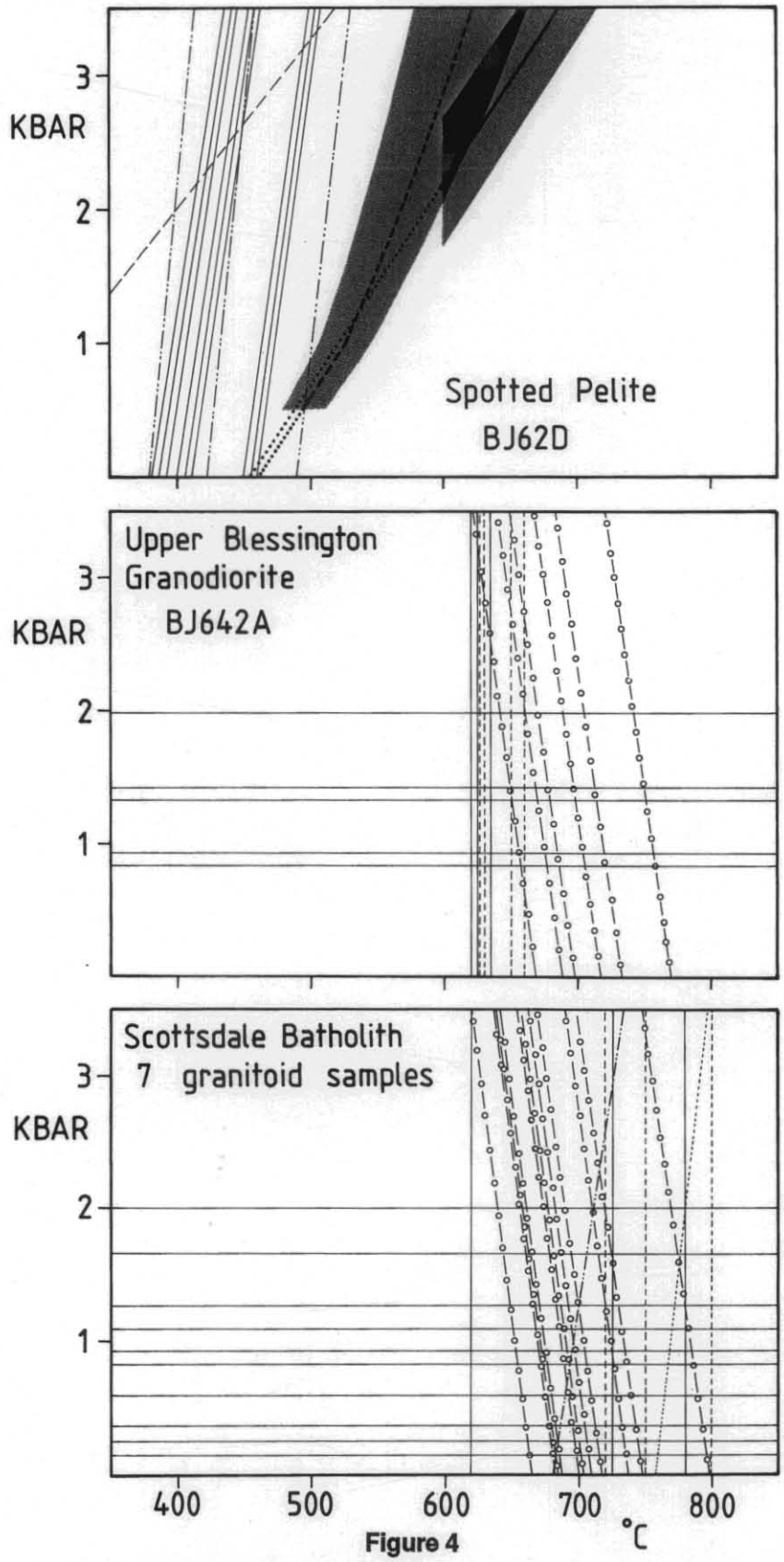

Figure 4

Plots of geothermometer, geobarometer and equilibrium thermodynamics calculations for the spotted pelite sample (BJ62D) and the Scottsdale Batholith granodiorites. Symbols are the same as in Figure 3, with the following additions:

dash double dotted	—	Two feldspar geothermometry
dash crossed line	—	Muscovite-plagioclase geothermometry
vertical solid line	—	Hornblende-clinopyroxene geothermometry
vertical dashed line	—	Biotite-clinopyroxene geothermometry
dash circled line	—	Hornblende-plagioclase geothermometry
horizontal solid line	—	Al in hornblende geobarometry

5 cm

equivalent to or slightly lower than the minimum temperature for granitic melt formation. Thus the above T estimates of the crystallisation of the Scottsdale Batholith are consistent with the lower temperature range of granitic melt formation at 1–2 kbar with fluid present; >750°C (Veielzeuf and Holloway, 1988), >680–700°C (Ebadi and Johannes, 1991) and >650–760°C (Peterson and Newton, 1990).

GEOBAROMETRY

The Si-cations in phengite (Cathelineau, 1988) and biotite-muscovite-K feldspar (Bucher-Nurminen, 1987) geobarometers have been applied to the spotted pelite samples (Tables 6 and 7, fig. 3 and 4). For a temperature estimate of 470°C the average results are 1860 bar and 1780 bar respectively for the phengite and bi-mu-kfd geobarometers. These two calibrations are very consistent with each other and with phase stability constraints (fig. 2), thus they are considered reliable estimates of pressure during contact metamorphism. The muscovite-biotite-chlorite geobarometer (Powell and Evans, 1983) yielded inconsistent and geologically unreasonable results as anticipated, because of the disequilibrium of the bi-mu-chl assemblage due to chlorite being a retrograde phase. As expected, there is no systematic variation in pressure estimates with respect to distance of the sample from the Scottsdale Batholith. The sample closest to the batholith (373C) also has the lowest P estimate. This variation, and the higher P estimate of sample BJ62D, cannot be considered real because these two extremes are encompassed within the error range for these methods (at least ± 500 bar).

Three calibrations of the Al in hornblende geobarometer for granodiorite whole-rock compositions have been applied to the Scottsdale Batholith samples (Table 8, fig. 4). These hornblendes are of ferro-hornblende chemistries with very low number of Al-cations (for 24 oxygen), ranging from 0.87 to 1.20 and averaging 1.03 cations. The hornblende compositions, the host assemblage (absence of garnet) and whole-rock compositions (granodiorite) are all entirely appropriate for the application of this geobarometer, which has been calibrated empirically and experimentally using similar rocks. The average pressures using the calibration of Hollister *et al.* (1987) are 1306 bar and 920 bar for sample BJ642A and the sum of SB samples respectively. These results are consistent with, though slightly lower than, pressure estimates from the spotted pelites. The higher pressures of sample BJ642A are not considered real, as the large error range for this geobarometer (± 1 kbar) encompasses the range in pressures between samples. Despite the large error range of this method the very low pressure results no doubt reflect very shallow depths of emplacement of the Scottsdale Batholith.

EQUILIBRIUM THERMODYNAMICS

Average P and average T calculations were derived using the equilibrium thermodynamics method of Powell and Holland (1988, 1985). This method employs an internally consistent thermodynamic dataset to solve the set of independent reactions that can be drawn up using the mineral endmembers in the sample studied. All calculations were performed using the program THERMOCALC v2.01β with the updated (1992) thermodynamic dataset. This method has been applied to three spotted metapelite samples with the following assemblages; and-cd-mu-bi-q ± kfd ± pl. Andalusite is identified in only one of these samples but is assumed to be in excess in all these samples. The reactions used in performing the calculations, and the resultant average pressures and temperatures, are presented in Table 9 and plotted in Figure 2.

For a pressure estimate of 1.2 kbar, the average temperature results are 545°C ± 25°C and 535°C ± 20°C. The small errors and satisfaction of the chi squared test for 95% confidence suggests that these are reliable temperature estimates. However, these results are approximately 60–80°C higher than those by bi-mu geothermometry. The temperature estimates by equilibrium thermodynamics are more consistent with the P-T field of stability of spotted metapelite assemblages (fig. 2) than estimates by bi-mu geothermometry. Thus equilibrium thermodynamics T estimates may reflect the T_{max} experienced, and the calibration of the bi-mu geothermometer may be low.

The results of average P calculations in samples 373N and BJ62D are consistent with the other P-T estimation methods employed (fig. 3, 4). However the results of sample 373J are meaningless. Combined with T estimates by either equilibrium thermodynamics or bi-mu and two feldspar geothermometry, the average P results are 0.75 and 1.25 kbar for 373N and BJ62D respectively (fig. 3, 4). These results are entirely consistent with pressures estimated by the geobarometers discussed above.

DISCUSSION

The preferred P-T loci for each sample (Table 10) have been obtained as the average of intersections of what are considered the most reliable P and T estimation methods (fig. 3, 4). These loci suggest that the metamorphic conditions in the thermal aureole at T_{max} were between 450°C and 545°C at pressures of 1.2 ± 0.45 kbar. The Scottsdale Batholith crystallised at 670–695°C while at 0.90–1.30 kbar pressure. Pressure estimates from both the granodiorites and the contact aureole are identical. Thus crustal pressure experienced at the time of batholith emplacement, by the rocks presently exposed, was 1.2 ± 0.45 kbar. This corresponds to a depth of 4.2 ± 1.6 km (Winkler, 1979). Such extremely shallow crustal levels of emplacement are compatible with the presence of coeval acidic extrusive rocks at St Marys. The geothermal gradient within the contact aureole at T_{max} was extremely high, being 107–130°C/km.

The crustal level, of rocks presently exposed, during the mega-kinking (D_2) deformational episode is considered to be ≤4.2 km depth, as there is no evidence for loading or crustal thickening subsequent to Devonian batholith intrusion (356–398 Ma). However, these same rocks were exposed before deposition of the Parmeener Supergroup at approximately 300 Ma. Thus during the period 356 to 300 Ma the northeast of Tasmania underwent mega-kinking deformation as well as approximately 4.2 km of uplift and denudation. If this denudation occurred continually from the time of batholith emplacement, the mega-kinking of rocks presently exposed must have occurred at crustal levels shallower than 4.2 km. This constraint on the

extremely shallow crustal level at which D_2 deformation occurred is entirely consistent with the style (sharp angular and "instantaneous" kinking) of deformation and its brittle nature. Furthermore, the vertical axes of the kink folds are consistent with insignificant crustal loads. The mega-kinking style of D_2 deformation in northeast Tasmania not only required shallow crustal levels but also required both:

(1) The pre-existence of the steeply-inclined grain of the terrain resulting from the pervasive penetrative D_1 cleavage.

(2) And a horizontal principle compressive stress (σ_1) directed along the length of this pre-existing structural grain.

In other terrains, where these two criteria are met, the development of large-scale kinkbands may well be the typical style of tectonics expected at extremely shallow crustal levels.

The T_{max} of the contact aureole spotted metapelites (450–545°C) is relatively low for contact aureloes around large granitoid batholiths, this being typically in the order of 600–700°C (Reverdatto, 1973; Bucher-Nurminen, 1982; Owen, 1991; Hover *et al.*, 1983). The low temperature of the Scottsdale Batholith aureole can be interpreted by three hypotheses.

(1) Calibrations of the geothermometers used may be low. This is not considered true because of the close correlation between the three calibrations used in this study. Geothermometer results are lower than T estimates by equilibrium thermodynamics, even so, the T_{max} of the latter method is only 545°C. Similarly the geothermometry estimates are not considered to be closure temperatures, in which the mineral pairs re-equilibrated with cooling until reaching some arbitary temperature. Re-equilibration of the mineral pairs subsequent to T_{max} is very unlikely to have occurred at such low temperatures because the kinetic energy available for re-equilibration would have been so low.

(2) The Scottsdale Batholith was intruded into extremely shallow crustal levels, thus the thin section of crustal overburden did not significantly impede the diffusion of heat to the surface. Consequently, the contact aureole thermal pulse was short lived and the geothermal gradient was so steep (107–130°C/km) that the thermal aureole was both cooler and narrower than a more deeply buried contact aureole would be (fig. 5). Such a hypothesis is supported by both the shallow crustal levels of emplacement (4.2 km) and also the large T gradient between the granodiorite and the thermal aureole (approximately 200°C) (fig. 5).

(3) Alternatively the Scottsdale Batholith was emplaced as a relatively cool magma body. This hypothesis is supported by the low crystallisation temperature estimates from the Scottsdale Batholith (670–695°C) with respect to the minimum temperature for granitic melt formation at 1–2 kbar with fluid present (>750°C, Veielzeuf and Holloway, 1988; >680–700°C, Ebadi and Johannes, 1991; and >650–760°C, Peterson and Newton, 1990). Furthermore, these minimum temperatures for granitic melt stability are significantly increased for water activities and for granodiorite melt compositions. Consequently the Scottsdale Batholith may have been emplaced as an already partially solidified and thus relatively cool granodiorite body.

The two alternative hypotheses (2 and 3 above) for the low temperature of contact metamorphism (relative to the intruding granitoid) are both consistent with the T and P estimates available for emplacement of the granitoid, and both are not mutually exclusive. To evaluate which of the two had the dominant control of T_{max} in the thermal aureole, a study involving thermal modelling of the contact aureole for intrusions of different temperatures and at different crustal levels is required.

Subsequent to contact metamorphism the aureole rocks presumably cooled very quickly to a more normal crustal geotherm. Rapid thermal re-equilibration is anticipated because the shallow crustal levels imply these rocks were not well insulated by a thick sequence of overlying rocks. The contact aureole rocks cooled rapidly and were possibly thermally equilibrated at a typical crustal geotherm of 25°C/km, this possibly being attained within <10 Ma of the time of intrusion (Peacock, in Spear and Peacock, 1990). The presently exposed Mathinna Beds resided at approximately 3.15–6.13 km depth during contact metamorphism and thus after thermal equilibration of the northeast Tasmanian crust, this crustal level experienced temperatures of only 79–153°C. These temperatures are consistent with the brittle nature of the kinking style of deformation that post-dated the granitoid intrusions.

REFERENCES

BANKS, M. R.; SMITH, E. A. 1968. A graptolite from the Mathinnna Beds, North-eastern Tasmania. *aust. J. Sci.* 31:118–119.

BLUNDY, J. D.; HOLLAND, T. J. B. 1990. Calcic amphibole equilibria and a new amphibole-plagioclase geothermometer. *Contr. Mineral. Petrology* 104:208–224.

BUCHER-NURMINEN, K. 1982. On the mechanism of contact aureole formation in dolomitic country rock by the Adamello intrusion (northern Italy). *am. mineral* 67:1101–1117.

BUCHER-NURMINEN, K. 1987. A recalibration of the chlorite-biotite-muscovite geobarometer. *Contr. Mineral. Petrology* 96:519–522.

BURNELL, J. R.; RUTHERFORD, M. J. 1984. An experimental investigation of the chlorite terminal equilibrium in pelitic rocks. *am. mineral.* 69:1015–1024

CATHELINEAU, M. 1988. Cation site occupancy in chlorites and illites as a function of temperature. *Clay Minerals* 23:471–485.

CHENEY, J. T.; GUIDOTTI, C. V. 1979. Muscovite-plagioclase equilibria in sillimanite + quartz bearing metapelites, Puzzle Mountain Area, northwest Maine. *am J. Sci.* 279:411–434.

COCKER, J. D. 1982. Rb-Sr geochronology and Sr isotopic composition of Devonian granitoids, eastern Tasmania. *J. geol. Soc. Aust.* 29:139–158.

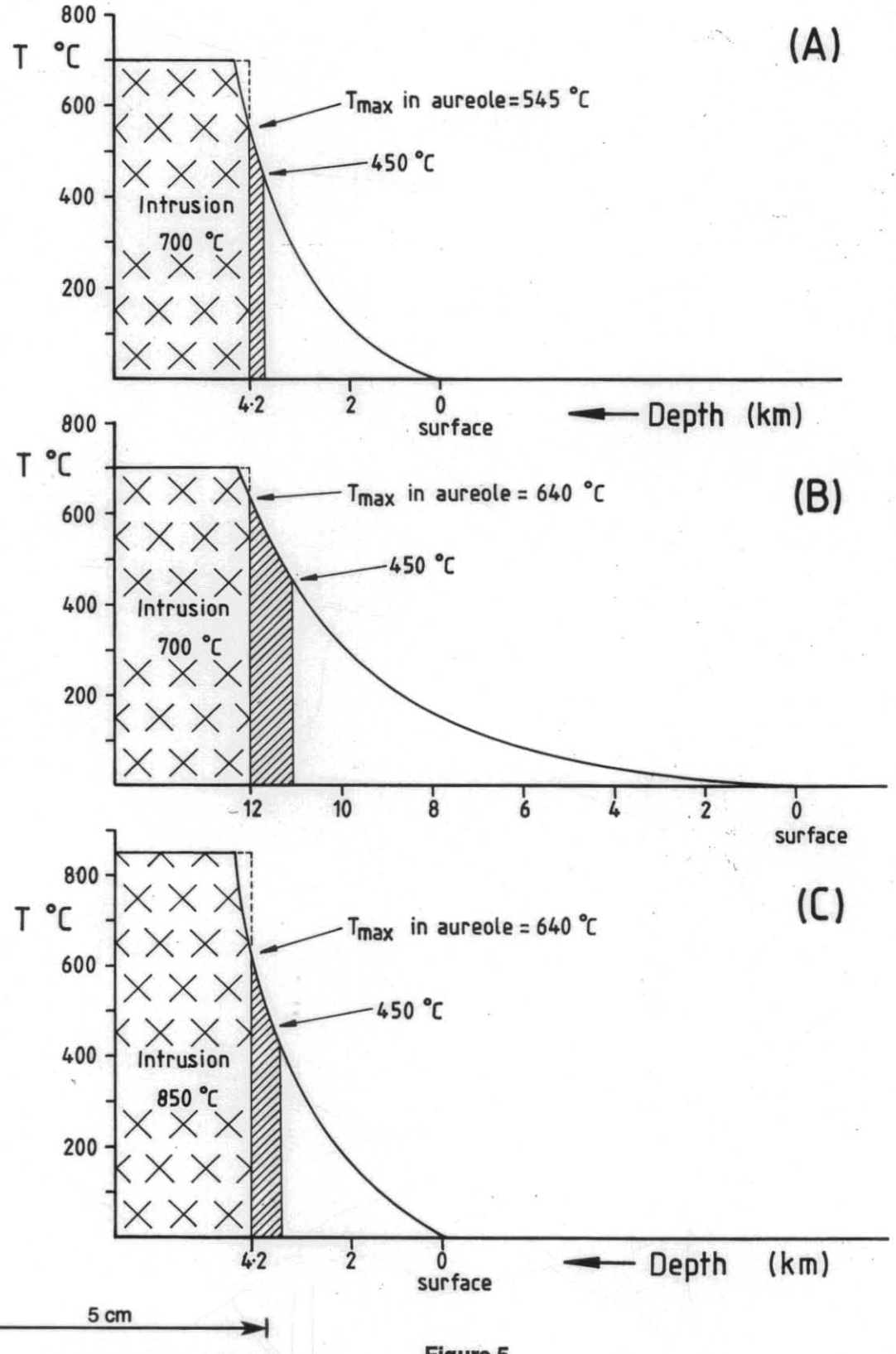

Figure 5

Idealised thermal profiles of contact aureoles, immediately after intrusion, with respect to crustal depth. These thermal profiles are only diagrammatic to illustrate the discussion in the text; they have not been modelled. For all examples the width of the contact aureole (shaded) is defined by the 450°C isotherm. Note postulated variations in T_{max} within the contact aureole and variations in the width of the aureole for different scenarios.

(A) Cool granitoid (700°C) intruded into very shallow crustal levels (4.2 km depth).

(B) Cool granitoid (700°C) intruded into intermediate crustal levels (12 km depth).

(C) Hot granitoid (850°C) intruded into very shallow crustal levels (4.2 km depth).

DEER, W. A.; HOWIE, R. A.; ZUSSMAN, J. 1966. *An introduction to the rock forming minerals.* Longman : London.

EBADI, A.; JOHANNES, W. 1991. Beginning of melting and composition of first melts in the system Qz-Ab-Or-H_2O-CO_2. *Contr. mineral. Petrology* 106:286–295.

GOSCOMBE, B. D.; FINDLAY, R. F. 1989. Mega-kinking in the Mathinna Beds, north-east Tasmania. *Rep. Dep. Mines Tasm.* 1989/42.

HAMMARSTROM, J. M.; ZEN, E-AN. 1986. Aluminium in hornblende: an empirical igneous geobarometer. *am. mineral.* 71:1297–1313.

HENSEN, B. J.; GREEN, D. H. 1973. Experimental study of cordierite and garnet in pelitic compositions at high pressures and temperatures. 3. Synthesis of experimental data and geological applications. *Contr. mineral. Petrology* 38:151–166.

HOISCH, T. D. 1989. A muscovite-biotite geothermometer. *am. mineral.* 74:565–572.

HOLDAWAY, M. J.; LEE, S. M. 1977. Fe-Mg cordierite stability in high-grade pelitic rocks based on experimental, theoretical and natural observations. *Contr. mineral. Petrology* 63:175–198.

HOLLISTER, L. S.; GRISSOM, G. C.; PETERS, E. K.; STOWELL, H. H.; SISSON, V. B. 1987. Confirmation of the empirical correlation of Al in hornblende with pressure of solidification of calc-alkaline plutons. *am. mineral.* 72:231–239.

HOVER GRANATH, V. C.; PAPIKE, J. J.; LABOTKA, T. C. 1983. The Notch Peak contact metamorphic aureole, Utah: Petrology of the Big Horse Limestone Member of the Orr Formation. *Bull. geol. Soc. Am.* 94:889–906.

JOHNSON, M. C.; RUTHERFORD, M. J. 1989. Experimental calibration of the aluminium-in-hornblende geobarometer with application to Long Valley caldera (California) volcanic rocks. *Geology* 17:837–841.

LAIRD, J. 1989. Chlorites; metamorphic petrology. *Reviews in mineralogy* 19:405–453.

MASSONE, H. -J. 1989. The upper thermal stability of chlorite + quartz: an experimental study in the system MgO-Al_2O_3-SiO_2-H_2O. *J. Met. Geol.* 7:567–581.

MASSONNE, H. -J.; SCHREYER, W. 1987. Phengite geobarometry based on the limiting assemblage with K-feldspar, phlogopite and quartz. *Contr. mineral. Petrology* 96:212–224.

MIYAKE, A. 1990. Dendritic cordierite in argillaceous hornfels from the Toki area, Gifu Prefecture, central Japan. *Contr. mineral. Petrology* 104:390–396.

OWEN, J. V. 1991. Cordierite + spinel parageneses in pelitic gneiss from the contact aureoles of the Mistastin batholith (Quebec) and the Taylor Brook gabbro complex (Newfoundland). *Can. J. Earth. Sci.* 28:372–381.

PERCHUK, L.L.; ARANOVICH, L. YA.; PODLESSKII, K. K.; LAVRENT'EVA, I. V.; GERASIMOV, V. YU.; FED'KIN, V. V.; KITSUL, V. I.; KARSAKOV, L. P.; BERDNIKOV, N. V. 1985. Precambrian granulites of the Aldan Shield, eastern Siberia, USSR. *J. Metamorphic Geol.* 3:265–310.

PETERSON, J. W.; NEWTON, R. C. 1990. Experimental biotite-quartz melting in the KMASH-CO_2 system and the role of CO_2 in the petrogenesis of granites and related rocks. *am. mineral.* 75:1029–1042.

POWELL, M.; POWELL, R. 1977. Plagioclase-alkali-feldspar geothermometry revisited. *Mineral. Mag.* 41:253–256.

POWELL, R.; EVANS, J. A. 1983. A new geobarometer for the assemblage biotite-muscovite-chlorite-quartz. *J. Met. Geol.* 1:331–336.

POWELL, R.; HOLLAND, T. J. B. 1985. An internally consistent thermodynamic dataset with uncertainties and correlations: 1. Methods and a worked example. *J. Met. Geol.* 3:327–342.

POWELL, R.; HOLLAND, T. J. B. 1988. An internally consistent dataset with uncertainties and correlations: 3. Applications to geobarometry, worked examples and a computer program. *J. Met. Geol.* 6:173–204.

POWELL, R.; HOLLAND, T. J. B. 1990. Calculated mineral equilibria in the pelite system, KFMASH (K_2O-FeO-MgO-Al_2O_3-SiO_2-H_2O). *am. mineral.* 75:367–380.

RAVERDATTO, V. V. 1973. *The facies of contact metamorphism.* Translated by D.A. Brown, Australian National University

RICKARDS, R. B.; BANKS, M. R. 1979. An Early Devonian monograptid from the Mathinna Beds, Tasmania. *Alcheringa.* 3:307–311.

SCHREYER, W.; MARESCH, W. V.; DANIELS, P.; WOLFSDORFF, P. 1990. Potassic cordierites: characteristic minerals for high-temperature, very low-pressure environments. *Contr. mineral. Petrology* 105:162–172.

SPEAR, F. S.; CHENEY, J. T. 1989. A petrogenetic grid for pelitic schists in the system SiO_2-Al_2O_3-FeO-MgO-K_2O-H_2O. *Contr. mineral. Petrology* 101:149–164.

SPEAR, F. S.; PEACOCK, S. M. 1990. *Program manual and computer exercises for the calculation of metamorphic phase equilibria, pressure-temperature-time paths and thermal evolution of orogenic belts.* Department of Geology, Rensselaer Polytechnic Institute, Troy, NY.

VIELZEUF, D.; HOLLOWAY, J. R. 1988. Experimental determination of the fluid-absent melting relations in the pelitic system. Consequences for crustal differentiation. *Contr. mineral. Petrology* 98:257–276.

VRY, J. K.; BROWN, P. E.; VALLEY, J. W. 1990. Cordierite volatile content and the role of CO_2 in high-grade metamorphism. *am. mineral.* 75:71–88.

WILLIAMS, E. 1970. Kink-bands developed during folding of sandstaone layers at Stony Head, Tasmania. *Tectonophysics.* 10:433–457.

WINKLER, H. G. F. 1979. *Petrogenesis of metamorphic rocks. 5th edition.* Springer-Verlag.

[20 December 1992]

ABBREVIATIONS FOR MINERALS AND MINERAL END MEMBERS

Mineral abbreviations		Mineral end member abbreviations	
q	quartz	crd	Mg-cordierite
cd	cordierite	fcrd	Fe-cordierite
and	andalusite	mu	muscovite end member
bi	biotite	cel	celadonite
mu	muscovite	ann	annite
pl	plagioclase	east	eastonite
kfd	K-feldspar	phl	phlogopite
chl	chlorite	naph	Na-phlogopite
ilm	ilmenite	san	sanidine
rut	rutile	an	anorthite
hem	hematite	ab	albite
cpx	clinopyroxene	pa	paragonite
hn	hornblende	or	orthoclase
act	actinolite		
ep	epidote		
ctd	chloritoid		
g	garnet		
as	alumino-silicate		
v	vapour		
ky	kyanite		
sill	sillimanite		

Table 1

Summary of the petrology of samples discussed in report

Sample	Distance from contact (m)†	and	cd	bi	mu	pl	kfd	q	chl	ilm	rut	pinite	cpx	hn	act	ep	sphene
Spotted pelites																	
373N*	80	I	X	X	X			X		X	X						
373C*	11			X	X			X	R								
373J*	45		X	XI	X		X	XI		X							
374*	200		XPs	XI	XR		X	XI		X	X	R					
376*	450		Ps	X#	XR			X	R	XR							
392*	1200		XPs	XI#	XI			XI	R	X							
373A	3		X	X	X			X		X	X						
373B	7		X	X	XR			X	R	X	X						
373C#2	11		X	X	XR			X	R	X							
373E	19		Ps	X	XR			X		X		R					
373G	30		XPs	X	XR			X	R	X		R					
378	770	X	XPs	X	XR			X		X							
BJ62D*	EQ470056		X	X	X	X	X	X									
Granodiorites																	
BJ642A*	EQ488054			X	X	X	X	X					X	X	X		
SB-21A*	EQ354215			X		X	X	X					X	X		X	
SB-18*	EQ392100			X		X	X	X		X				X			
SB-4*	EQ540497			X		X	X	X	X					X			
SB-1	EQ439479			X		X		X						X			
SB-5*	EQ552411			X		X	X	X						X			
SB-12*	EQ520207			X		X		X						X			
SB-20	EQ586278			X		X		X		X							
SB-19	EQ569375			X		X	X	X									
SB-14*	EQ595219			X		X	X	X						X			
SB-2	EQ417401			X		X		X									
SB-13	EQ573222			X		X	X	X	X								X

† Distance or AMG grid reference

* Minerals have been analysed and P-T conditions of formation estimated

X Mineral present in matrix of sample

I Inclusion phase within poikiloblastic cordierite

Ps Cordierite porphyroblast has been pseudomorphed

R Retrograde mineral

\# Biotite-chlorite interlayered mixtures

Table 2

Biotite-muscovite geothermometry (Hoisch, 1989), in °C, errors ± 50°C.

Sample	Biotite	Muscovite	1 kbar	2 kbar	3 kbar
BJ62D	c1#5	c3#1	463	478	492
	c1#6	c3#1	468	482	496
	c1#2	c3#1	472	486	500
	c1#5	c2#1	415	431	446
	c1#6	c2#1	421	436	451
	c1#2	c2#1	425	440	455
	c1#5	c2#2	396	412	428
	c1#6	c2#2	402	418	433
	c1#2	c2#2	407	423	438
373N	c1#1	c1	439	454	469
	c1#2	c1	440	455	471
	c2	c2 lath	457	471	486
	c1#1	c1 lath	437	452	467
	c1#2	c1 lath	438	453	468
373C	c3#1	c2	428	444	460
	c3#2	c2	428	444	460
	c3#3	c2	429	445	461
373J	in cd#1	in cd	443	458	473
	in cd#2	by cd	452	467	482
	matrix	at#2	445	460	476
	matrix	core	466	481	496
374	matrix	matrix	464	479	493
	fine	musc	430	446	461
	lath#1	lath#1	454	468	483
	Fe-rich	matrix	422	439	455
	lath#2	lath#2	430	445	461
376	c2 real	c2#3	665*	676*	686*
	c2 real	c2#1	670*	681*	691*
	c2 real	c2#2	782*	791*	800*
392	c1#1	c1#1	674*	683*	693*
	c2#1	c2#1	700*	710*	719*
	c2#1	c2#2	697*	706*	716*
	c2#1	c3 after cd	688*	698*	708*
	c2#1	c3 matrix	689*	700*	710*

* The mineral pair is not in equilibrium, muscovite may have re-equilibrated during cooling

Table 3

Plagioclase – K-feldspar (Powell and Powell, 1977) and plagioclase-muscovite (Cheney and Guidotti, 1979) geothermometry, in °C

Sample	Plagioclase	K-feldspar	Muscovite	1 kbar	2 kbar	3 kbar
Plagioclase – K-feldspar geothermometry						
BJ62D	c1#7	c3#4	-	501	512	524
	c1#7	c3#5	-	433	443	453
	c1#7	c3#6	-	389	399	409
	c1#7	c3#7	-	501	512	523
SB-18	c1#1	c2#1	-	859	875	892
SB-19	c1#1	c5#1	-	698	712	726
BJ642A	all	all	-	<384*	<394*	<403*
SB-21A	all	all	-	<487*	<498*	<509*
SB-4	all	all	-	<295*	<303*	<312*
*Plagioclase-muscovite geothermometry***						
BJ62D	c1#7	-	c3#1	445	449	452
	c1#7	-	c2#1	457	460	464
	c1#7	-	c2#2	459	462	466

* The mineral pairs are not in equilibrium, the composition of the feldspars may have been re-equilibrated during cooling by exsolving perthitic lamelli

** Geothermometer was calibrated empirically using sillimanite-bearing assemblages. Assumed $fH_2O = 6.95$

Table 4

Biotite-chlorite (Dickenson; *in* Laird, 1989) and chlorite (Cathelineau, 1988) geothermometry, in °C

			Biotite-Chlorite			Chlorite
Sample	Biotite	Chlorite	1 kbar	2 kbar	3 kbar	
373C	c3#2	c2#2	612*	622*	632*	395**
	c3#3	c2#3	537*	546*	555*	389**
	c1	c1	360*	367*	374*	289**
	c3#1	c2#1	745*	757*	768*	399**
376	c2 real	c2#2	277*	283*	289*	382**
	c2 real	c2#3	290*	296*	302*	408**
SB-4	c2#2	c3#3	768*	780*	792*	205**
392	-	all	-	-	-	<231**

* The mineral pair is not in equilibrium; chlorite may be retrogressive or has re-equilibrated during cooling

** Chlorite may be retrograde

Table 5

Biotite-clinopyroxene and hornblende-clinopyroxene (Perchuk *et al.*, 1985) and hornblende-plagioclase (Blundy and Holland, 1990) geothermometry, in °C

Sample	Horn	Plag	Biotite	Cpx	Horn-Plag* 1 kbar	Horn-Plag* 2 kbar	Horn-Plag* 3 kbar	Hn-Cpx	Bi-Cpx
BJ642A	c4#1	c7#3	c1#2	c1#1	674	660	647	620	630
	c4#3	c4#4	c3#1	c5#1	755	741	726	635	650
	c4#5	c5#5	c3#4	c6#1	655	642	629	625	625
	c4#1	c2#1	-	-	702	688	674	-	-
	c4#3	c3#5	-	-	718	704	690	-	-
	c4#5	c3#6	-	-	683	669	656	-	-
	-	-	c3#3	c6#2	-	-	-	-	660
	-	-	c8#2	c6#1	-	-	-	-	630
SB-21A	c6#2	-	c5#3	c5#1	-	-	-	725	750
	c6#3	-	c9#1	c9#2	-	-	-	620	720
	c1#3	c2c	c1#4	c1#2	724	710	696	780	800
	c1#3	c2r	-	-	733	719	705	-	-
SB-4	c3#1	c5#1	-	-	703	689	675	-	-
	c3#1	c2#1	-	-	669	656	643	-	-
SB-18	c3#1	c1#1	-	-	784	770	755	-	-
SB-5	c2#1	c4#2r	-	-	674	661	647	-	-
	c2#1	c4#3c	-	-	690	676	663	-	-
SB-12	c3#1	c5#1	-	-	670	657	644	-	-
	c4#2	c5#1	-	-	652	639	626	-	-
SB-14	c5#1	c6#1	-	-	688	675	661	-	-
	c4#1	c2#1	-	-	696	682	668	-	-

* Used T2 of Blundy and Holland (1990) for X_{ab} in plagioclase >0.5. Error is ± 75°C

Table 6

Si in phengite geobarometry for limiting assemblage mu-kfd-bi-q (Massone and Schreyer, 1987). Error ≥ ± 500 bar

Sample	Si-cations in muscovite ave.	Si-cations in muscovite range	Pressure in kbar at 550°C ave.	Pressure in kbar at 550°C range	Pressure in kbar at 400°C ave.	Pressure in kbar at 400°C range
373N*	3.07	(3.07–3.08)	3.0	(3.0–3.3)	1.1	(1.1–1.4)
373C*	3.02	(2.97–3.07)	1.7	(0.2–3.0)	0.0	(<<0–1.1)
373J	3.05	(3.04–3.06)	2.4	(2.1–2.7)	0.7	(0.5–0.9)
374	3.05	(3.01–3.09)	2.4	(1.2–3.3)	0.7	(-0.5–1.4)
376*	3.10	(3.04–3.16)	3.6	(2.1–4.8)	1.7	(0.5–3.0)
392*	3.06	(3.04–3.10)	2.7	(2.1–3.6)	0.9	(0.5–1.7)
BJ62D	3.11	(3.11–3.12)	3.9	(3.9–4.2)	2.0	(2.0–2.3)

* K-feldspar has not been identified in sample

Table 7

Biotite – muscovite – K-feldspar geobarometry (Bucher-Nurminen, 1987). Error ± 500 bar

Sample	Biotite	Muscovite	K-feldspar	Pressure in kbar at 400°C	Pressure in kbar at 600°C
373J	in cd#1	in cd	core	1.1	2.6
	in cd#2	by cd	core	1.7	2.8
374	lath#1	lath#1	kfd#1	1.1	2.6

Table 8

Al in hornblende geobarometry for limiting whole-rock granodiorite compositions (pressure in bars)

Sample		Al-cations in horn (24 oxygen)	Hammarstrom and Zen, 1986 (± 3 kbar)	Hollister *et al.*, 1987 (± 1 kbar)	Johnson and Rutherford, 1989 (± 0.5 kbar)
BJ642A	c4#1	0.993	1072	838	738
	c4#3	1.197	2102	1993	1605
	c4#5	1.010	1162	939	814
	c5#2	1.078	1503	1321	1101
	c7#1	1.098	1604	1434	1185
	average		1489	1305	1089
SB-21A	c6#2	1.04	1311	1106	939
	c4#1	1.01	1160	936	812
	c3#2	1.14	1814	1670	1362
	c1#3	0.95	859	598	559
SB-18	c3#1	1.20	2116	2008	1616
SB-4	c3#1	0.89	557	260	305
SB-5	c2#1	0.91	657	372	389
SB-12	c3#1	0.87	456	147	220
SB-14	c5#1	1.07	1462	1275	1066
	c4#1	0.99	1060	824	728
all SB	average		1145	920	800

Table 9

Results of P-T estimates by the equilibrium thermodynamics method of Powell and Holland (1988) using the 1992 version of the program THERMOCALC v2.0β. In all samples coexisting fluid is assumed to be pure water (X_{H_2O} = 1.0). f is the chi squared test, for 95% confidence f<1.54–1.63.

Sample	Mineral end-members used	Ave. P calculations			Ave. T calculations		
		T est. (°C)	P result (kbar)	f	P est. (kbar)	T result (°C)	f
373J*	crd, fcrd, q, H_2O, and, mu, cel, pa, ann, phl, naph, san, ab	600	0.6 ± 0.37	1.9	0.5	503 ± 21	1.2
		700	3.0 ± 0.21	0.5	1.0	535 ± 25	1.3
					2.0	579 ± 32	1.4
					3.0	617 ± 38	1.6
					4.0	653 ± 44	1.8
373N	crd, fcrd, q, H_2O, and, mu, cel, pa, ann, phl, naph	400	<0.5 ± 0.75	1.8			
		500	1.2 ± 0.55	1.2			
		600	2.0 ± 0.51	0.7			
		700	2.9 ± 0.57	0.4			
BJ62D*	crd, fcrd, q, H_2O, and, mu, cel, pa, ann, phl, east, san, ab	600	2.2 ± 0.48	1.2	0.5	494 ± 17	0.8
		700	3.7 ± 0.45	0.3	1.0	525 ± 20	1.1
					2.0	568 ± 30	1.4
					3.0	605 ± 39	1.7
					4.0	639 ± 47	2.0

* Andalusite considered in excess although not identified in the sample

The sets of independent reactions used in average P and average T calculations.

Sample	For average P calculations	For average T calculations
373N	4and + 2cel = crd + q + 2mu 5crd + 9mu = 18and + 8cel + east 5crd + 8mu = 18and + 7cel + phl 7crd + 3fcrd + 16mu = 36and + 14cel + 2ann	
373J	4and + 2cel = crd + q + 2mu 5crd + 8mu = 18and + 7cel + phl 3and + 2cel = crd + H_2O + mu + san 7crd + 3fcrd + 16mu = 36and + 14cel + 2ann 4and + 2cel + 2ab = crd + q + 2pa + 2san	4mu + 2cel = 5H_2O + 3and + east + 5san 6mu + 2phl = 5H_2O + 3and + 3east + 5san cel + 5pa + phl = 5H_2O + 3and + 2east + 5ab
BJ62D	5crd + 9mu = 18and + 8cel + east 7q + 8and + 2ann = 3fcrd + 2mu 3crd + 2san + 2pa = 7q + 8and + 2phl + 2ab 3and + 2cel + pa = crd + H_2O + 2mu + ab	4mu + 2cel = 5H_2O + 3and + east + 5san 3mu + 3cel = 5H_2O + 3and + phl + 5san

Table 10

Summary of the preferred P and T of formation of each sample. Range of geothermobarometry estimates are given; this range is not the analytical error range

Sample	Methods used to define P-T loci	Temperature (°C)	Pressure (kbar)	Confidence in P-T loci
SPOTTED PELITES				
BJ62D	All methods	500 ± 85	1.70 ± 1.25	reliable
	Equil. Thermo.	540	1.25	
	Geo-T and Geo-P	440	2.50	
373C	Geo-T and Geo-P	490 ± 45	1.00 ± 1.00	
373J	Geo-T and Geo-P	467 ± 15	1.75 ± 0.40	reliable
373N	Equil... and Geo-P-T	450 ± 10	1.20 ± 0.50	reliable
	Equil... and Geo-T	450 ± 10	0.75 ± 0.50	
374	Geo-T and Geo-P	450 ± 25	1.35 ± 0.20	reliable
376*	Geo-T and Geo-P	-	2.50 ± 1.00	
392*	Geo-T and Geo-P	-	1.80 ± 0.60	
GRANODIORITES				
BJ642A	Geo-T and Geo-P	650 ± 40	1.30 ± 0.70	reliable
SB (all)	Geo-T and Geo-P	700 ± 80	0.92 ± 1.00	reliable

* Mineral phases in sample are not in equilibrium

APPENDIX 1

Representative mineral analyses

Representative analyses from the spotted pelites in the Scottsdale Batholith contact aureole and from granodiorites in the same batholith. Each analysis is labelled by the circle on the thin section that the analysis is from (i.e. c1#2 denotes second analysis in circle 1). Analysis conditions are discussed in the text. A dash denotes where it is not known if this element was analysed for, or is inapplicable.

	cd 373N c1#1	cd 373J core	cd 373J rim	cd BJ62D c3#3	and 373N core	bi 373N c1#1	bi 373J incd	bi 373J matrix	bi 374 lath2	bi 373C c3#2
SiO_2	48.14	47.09	47.40	49.82	37.63	35.35	34.22	34.11	33.70	35.65
TiO_2	0.00	0.08	0.07	-	0.00	2.53	2.95	2.59	2.87	2.38
Cr_2O_3	0.00	0.09	0.12	-	0.00	0.14	0.26	0.22	0.19	0.00
Al_2O_3	33.05	32.71	31.95	33.60	62.25	20.02	19.44	19.19	19.75	18.82
Fe_2O_3	0.72	1.79	1.31	-	-	3.62	3.45	3.48	3.60	3.30
FeO	10.10	9.21	9.49	7.98	0.26	18.47	17.57	17.76	18.38	16.80
MnO	0.14	0.12	0.17	0.44	0.00	0.10	0.08	0.01	0.02	0.11
MgO	6.86	6.87	7.00	8.10	0.00	7.30	7.27	7.50	7.20	8.76
CaO	0.02	0.05	0.05	-	0.00	0.00	0.07	0.05	0.05	0.11
Na_2O	0.22	0.23	0.21	-	0.00	0.13	0.13	0.15	0.12	0.16
K_2O	0.00	0.08	0.08	0.25	0.00	8.81	8.89	8.73	8.42	8.73
H_2O	-	-	-	-	-	3.99	3.90	3.87	3.89	3.95
Total	99.26	98.32	97.86	100.25	100.14	100.46	98.22	97.66	98.18	98.77
Si	4.96	4.91	4.97	5.03	1.01	2.66	2.63	2.64	2.60	2.71
Ti	0.0	0.01	0.01	-	0.00	0.14	0.17	0.15	0.17	0.14
Cr	0.0	0.01	0.01	-	0.00	0.01	0.02	0.01	0.01	0.00
Al	4.02	4.02	3.95	4.00	1.98	1.77	1.76	1.75	1.80	1.68
Fe^{3+}	0.06	0.14	0.10	-	-	0.20	0.20	0.20	0.21	0.19
Fe^{2+}	0.87	0.80	0.83	0.67	0.01	1.16	1.13	1.15	1.19	1.07
Mn	0.01	0.01	0.02	0.04	0.00	0.01	0.00	0.00	0.00	0.01
Mg	1.05	1.07	1.09	1.23	0.00	0.82	0.83	0.87	0.83	0.99
Ca	0.00	0.01	0.01	-	0.00	0.00	0.01	0.00	0.00	0.01
Na	0.04	0.05	0.04	-	0.00	0.02	0.02	0.02	0.02	0.02
K	0.00	0.01	0.01	0.03	0.00	0.85	0.87	0.86	0.83	0.85
OH	-	-	-	-	-	2.00	2.00	2.00	2.00	2.00

	bi BJ62D c1#2	mu 373N c1lath	mu 373J incd	mu 373J bycd	mu 374 lath	mu 373C c1	mu 376 c2#2	mu 392 c1#2	mu BJ62D c3#1
SiO_2	36.50	46.88	45.36	45.80	45.70	43.75	46.94	45.94	45.96
TiO_2	2.44	0.79	0.58	0.39	1.01	0.00	0.15	0.26	0.72
Cr_2O_3	-	0.00	0.08	0.17	0.16	0.00	0.00	0.00	0.00
Al_2O_3	19.92	36.22	36.02	36.31	35.97	30.96	32.72	36.89	32.93
Fe_2O_3	3.02	0.66	0.77	0.66	0.62	4.50	1.87	0.55	2.20
FeO	15.39	0.40	0.46	0.40	0.37	2.70	1.12	0.33	1.32
MnO	-	0.00	0.00	0.00	0.00	0.06	0.00	0.00	0.00
MgO	9.00	0.54	0.59	0.60	0.58	4.04	1.36	0.38	0.58
CaO	0.00	0.00	0.00	0.00	0.00	0.00	0.10	0.00	0.00
Na_2O	0.00	0.53	0.61	0.58	0.55	0.51	0.71	1.18	0.32
K_2O	9.47	10.37	9.72	9.97	9.71	9.39	8.82	8.96	10.38
H_2O	4.02	4.58	4.48	4.51	4.51	4.42	4.46	4.52	4.43
Total	99.76	100.97	98.68	99.39	99.18	100.33	98.26	99.02	98.84
Si	2.72	3.07	3.04	3.04	3.04	2.97	3.16	3.05	3.11
Ti	0.14	0.04	0.03	0.02	0.05	0.00	0.01	0.01	0.04
Cr	-	0.00	0.00	0.01	0.01	0.00	0.00	0.00	0.00
Al	1.75	2.80	2.84	2.85	2.82	2.48	2.60	2.88	2.63
Fe^{3+}	0.17	0.03	0.04	0.03	0.03	0.23	0.09	0.03	0.11
Fe^{2+}	0.96	0.02	0.03	0.02	0.02	0.15	0.06	0.02	0.07
Mn	-	0.00	0.00	0.00	0.00	0.00	0.00	0.00	0.00
Mg	1.00	0.05	0.06	0.06	0.06	0.41	0.14	0.04	0.06
Ca	0.00	0.00	0.00	0.00	0.00	0.00	0.01	0.00	0.00
Na	0.00	0.07	0.08	0.07	0.07	0.07	0.09	0.15	0.04
K	0.90	0.87	0.83	0.85	0.82	0.81	0.76	0.76	0.90
OH	2.00	2.00	2.00	2.00	2.00	2.00	2.00	2.00	2.00

	kfd 373J c2core	kfd 373J c2rim	kfd 374 #2	kfd BJ62D c3#5	pl BJ62D c1#7	ilm 373N c1#1	ilm-hm 373J c2	chl 373C c1	chl 376 c2#3	chl+mu 392 c1#3
SiO_2	64.46	63.92	63.85	65.85	67.78	0.09	0.19	27.81	23.84	36.42
TiO_2	0.36	0.27	0.24	-	-	51.45	51.06	0.54	0.08	0.34
Cr_2O_3	0.14	0.18	0.11	-	-	0.07	0.58	0.00	0.00	0.03
Al_2O_3	18.66	18.60	18.66	19.03	24.08	0.00	0.00	20.10	23.17	27.30
Fe_2O_3	0.10	0.10	0.31	-	-	0.00	1.05	4.31	4.17	2.43
FeO	-	-	-	-	-	44.97	44.44	21.98	21.28	12.38
MnO	0.02	0.00	0.01	-	-	1.21	0.96	0.00	0.16	0.04
MgO	0.00	0.00	0.01	-	-	0.00	0.10	11.93	13.28	6.79
CaO	0.00	0.00	0.00	0.00	3.41	0.01	0.43	0.02	0.03	0.05
Na_2O	2.24	2.11	1.34	1.71	10.06	0.00	0.01	0.05	0.03	0.05
K_2O	12.98	13.02	14.18	13.70	0.13	0.04	0.33	1.09	0.05	0.86
H_2O	-	-	-	-	-	-	-	11.46	11.25	12.47
Total	98.96	98.19	98.71	100.29	105.46	97.84	99.14	99.30	97.33	99.15
Si	2.98	2.98	2.97	3.00	2.83	0.00	0.00	2.91	2.54	3.50
Ti	0.01	0.01	0.01	-	-	1.00	0.98	0.04	0.01	0.02
Cr	0.01	0.01	0.00	-	-	0.00	0.01	0.00	0.00	0.00
Al	1.02	1.02	1.02	1.02	1.19	0.00	0.00	2.48	2.91	3.10
Fe^{3+}	0.00	0.00	0.01	-	-	0.00	0.02	0.34	0.33	0.18
Fe^{2+}	-	-	-	-	-	0.97	0.95	1.92	1.90	1.00
Mn	0.00	0.00	0.00	-	-	0.03	0.02	0.00	0.01	0.00
Mg	0.00	0.00	0.00	-	-	0.00	0.00	1.86	2.11	0.97
Ca	0.00	0.00	0.00	0.00	0.15	0.00	0.01	0.00	0.00	0.00
Na	0.20	0.19	0.12	0.15	0.81	0.00	0.00	0.01	0.01	0.01
K	0.76	0.77	0.84	0.80	0.01	0.00	0.01	0.15	0.01	0.11
OH	-	-	-	-	-	-	-	8.00	8.00	8.00

	hn BJ642A c4#3	hn BJ642A c4#5	hn SB21A c4#1	hn SB21A c6#2	pl BJ642A c5#5	pl SB21A core	cpx BJ642A c6#1	cpx SB21A c9#2	bi BJ642A c3#4	bi SB21A c9#1
SiO_2	46.68	48.06	49.15	48.38	67.66	57.69	51.62	52.72	35.64	36.86
TiO_2	1.25	1.06	0.95	0.95	-	-	-	-	4.44	4.20
Cr_2O_3	0.00	0.00	0.00	0.00	-	-	-	-	-	-
Al_2O_3	6.73	5.76	6.11	5.83	20.58	27.00	0.64	0.61	13.83	14.32
Fe_2O_3	3.33	3.45	2.79	2.66	-	-	-	0.71	3.97	3.41
FeO	16.97	17.61	14.21	13.56	-	-	15.11	11.59	20.22	17.40
MnO	0.50	0.70	0.41	0.31	-	-	0.81	0.66	0.28	0.00
MgO	9.60	10.14	12.98	13.00	-	-	9.75	12.62	9.57	11.43
CaO	11.72	11.43	11.56	11.37	1.17	9.10	22.08	22.08	0.53	0.00
Na_2O	0.86	0.98	0.93	0.84	10.46	5.77	-	-	-	-
K_2O	0.72	0.62	0.62	0.53	0.12	0.33	-	-	7.98	9.35
H_2O	2.00	2.03	2.07	2.03	-	-	-	-	3.92	4.00
Total	100.36	101.85	101.78	99.46	99.99	99.89	100.01	100.99	100.38	100.97
Si	6.99	7.09	7.11	7.14	2.95	2.58	1.99	1.98	2.72	2.76
Ti	0.14	0.12	0.10	0.11	-	-	-	-	0.26	0.24
Cr	0.00	0.00	0.00	0.00	-	-	-	-	-	-
Al	1.19	1.00	1.04	1.01	1.06	1.43	0.03	0.03	1.25	1.27
Fe^{3+}	0.37	0.38	0.30	0.30	-	-	-	0.02	0.23	0.19
Fe^{2+}	2.12	2.17	1.72	1.67	-	-	0.49	0.36	1.29	1.09
Mn	0.06	0.09	0.05	0.04	-	-	0.03	0.02	0.02	0.00
Mg	2.14	2.23	2.80	2.86	-	-	0.56	0.71	1.09	1.28
Ca	1.88	1.81	1.79	1.80	0.05	0.44	0.91	0.89	0.04	0.00
Na	0.25	0.28	0.26	0.24	0.89	0.50	-	-	-	-
K	0.14	0.12	0.11	0.10	0.01	0.02	-	-	0.78	0.89
OH	2.00	2.00	2.00	2.00	-	-	-	-	2.00	2.00

APPENDIX 2

The P-T dependence of cordierite-biotite Fe-Mg exchange

An evaluation of the potential for an empirically calibrated geothermometer and/or geobarometer based on Fe-Mg exchange between coexisting biotite and cordierite is presented here. The Fe-Mg exchange reaction between biotite and cordierite is;

$$0.5\ \text{Mg-cordierite} + 0.397\ \text{Fe-biotite} = 0.5\ \text{Fe-cordierite} + 0.397\ \text{Mg-biotite}$$

The distribution coefficient for this reaction is given by;

$$Kd = [(X_{Fe})^{cd} (X_{Mg})^{bi}] / [(X_{Mg})^{cd} (X_{Fe})^{bi}] \qquad \text{(Holdaway and Lee, 1977).}$$

Fe-Mg distribution coefficients for coexisting biotite-cordierite pairs have been calculated from mineral analyses in the literature and for the spotted metapelites discussed in this report (Table 11). These Kd are plotted against the published P and T estimates of formation of the respective samples (fig. 6). Linear relationships exist between Kd and both T and P. These relationships are given by;

$$T\ (°C) = (Kd - 0.776) / -0.00037$$
$$P\ (kbar) = (Kd - 0.612) / -0.019$$

P and T estimates from the spotted metapelite samples from northeast Tasmania exert a lot of influence on the fit of these linear solutions to the Kd data because there are no other bi-cd pairs in the literature that equilibrated at such low T and P.

The range in Kd is very small (0.45 to 0.61) for the large range of metamorphic conditions in which bi-cd assemblages form (450–850°C, 1–8.5 kbar). This is; $\Delta Kd = 0.004$ per $\Delta T = 10°C$, and $\Delta Kd = 0.02$ per $\Delta P = 1$ kbar. Consequently these linear solutions cannot be considered generally applicable for P and T estimation unless mineral analyses, and thus Kd, are very accurately known. As electron microprobe analytical errors are typically ± 0.01 wt%, the error on Kd is in the order of ± 0.05. Taking an error of ± 50°C for the temperature estimates from the literature and the pressure errors at ± 0.75 kbar, the resultant P and T errors for solutions to the above relationships are an absolute minimum of ± 75°C and ± 1 kbar. These error ranges encompass a large range of the geologically plausible Kd values, thus Fe-Mg exchange between biotite and cordierite cannot be considered useful as either a geothermometer or geobarometer.

REFERENCES

BICKLE, M. J.; ARCHIBALD, N. J. 1984. Chloritoid and staurolite stability: implications for metamorphism in the Archaean Yilgarn Block, Western Australia. *J. metamorph. Geol.* 2:179–203.

CLARKE, G. L.; COLLINS, W. J.; VERNON, R. H. 1990. Successive overprinting granulite facies metamorphic events in the Anmatjira Range, central Australia. *J. metamorph. Geol.* 8:65–88.

GOSCOMBE, B. D. 1989. *Structure and metamorphism of the northeast Strangways Range, N.T.* Ph.D. thesis, University of Melbourne.

HOLDAWAY, M. J.; LEE, S. M. 1977. Fe-Mg cordierite stability in high-grade pelitic rocks based on experimental, theoretical and natural observations. *Contr. mineral. Petrology* 63:175–198.

HUDSON, N. F. C. 1980. Regional metamorphism of some Dalradian pelites in the Buchan area, N.E. Scotland. *Contrib. mineral. Petrol.* 73:39–51.

PERCHUK, L.; GERYA, T.; NOZHKIN, A. 1989. Petrology and retrograde P-T path in granulites of the Kanskaya formation, Yenisey range, Eastern Siberia. *J. metamorph. Geol.* 7:599–617.

VAN REENEN, D. D. 1986. Hydration of cordierite and hypersthene and a description of the retrograde orthoamphibole isograde in the Limpopo belt, South Africa. *Am. mineral.* 71:900–915.

SANDIFORD, M. 1985. The origin of retrograde shear zones in the Napier Complex: implications for the tectonic evolution of Enderby Land, Antarctica. *J. Struct. Geol.* 7:477–488.

SHIBA, M. 1988. Metamorphic evolution of the southern part of the Hidaka belt, Hokkaido, Japan. *J. metamorph. Geol.* 6:273–296.

STÜWE, K.; POWELL, R. 1989. Low-pressure granulite facies metamorphism in the Larsemann Hills area, East Antarctica; petrology and tectonic implications for the evolution of the Prydz Bay area. *J. metamorph. Geol.* 7:465–483.

TUISKU, P.; LAAJOKI, K. 1990. Metamorphic and structural evolution of the Early Proterozoic Puolankajärvi Formation, Finland — II. The pressure-temperature-deformation-composition path. *J. metamorph. Geol.* 8: 375–391.

Table 11

Distribution coefficient for Fe-Mg exchange between coexisting biotite and cordierite. Data from literature with P and T estimates of the conditions of formation by the respective authors.

Author		$(X_{Fe})^{cd}$	$(X_{Fe})^{bi}$	Kd	P(kbar)	T(°C)
This report	BJ62D	0.3552	0.4891	0.5726	1.2	500
	373N	0.4585	0.5824	0.6071	1.2	500
	373J	0.4391	0.5648	0.6033	1.2	500
Holdaway and Lee, 1977				0.5630	3.0	600
				0.530	6.0	675
				0.512	4.0	800
				0.559	3.0	800
				0.5310	3.0	700
				0.5420	4.5	725
				0.5430	6.0	750
Stuwe and Powell, 1989		0.1799	0.3951	0.3359	4.5	750
Perchuk *et al.*, 1989		0.2610	0.3930	0.5455	3.0	620
		0.2050	0.4030	0.3819	4.4	700
		0.1880	0.2920	0.5614	4.6	680
		0.1760	0.3540	0.3898	6.0	790
		0.1930	0.3490	0.4460	6.0	790
Clarke *et al.*, 1990		0.4300	0.6000	0.5029	2.5	750
Goscombe, 1989		0.1342	0.2399	0.4956	8.0	850
		0.1319	0.2654	0.4206	8.0	850
		0.1683	0.3139	0.4423	8.0	850
		0.0826	0.1562	0.4864	8.0	850
Hudson, 1980		0.4607	0.5991	0.5716	3.0	600
		0.4322	0.5690	0.5766	3.0	600
		0.3989	0.5245	0.6016	3.0	600
		0.4278	0.5496	0.6127	3.0	600
Shiba, 1988		0.3800	0.5600	0.4816	2.25	575
		0.3700	0.5400	0.5003	2.75	625
Sandiford,1985				0.4810	3.0	600
				0.6696	3.0	600
Bickle and Archibald, 1984		0.2538	0.3715	0.5754	4.2	545
		0.3190	0.4895	0.4885	4.2	545
Tuisku and Laajoki, 1990		0.1823	0.2919	0.5409	3.5	550
Van Reenen, 1986		0.1300	0.2700	0.4040	6.0	635
		0.1700	0.2800	0.5267	6.0	635
		0.1100	0.2200	0.4382	6.0	635

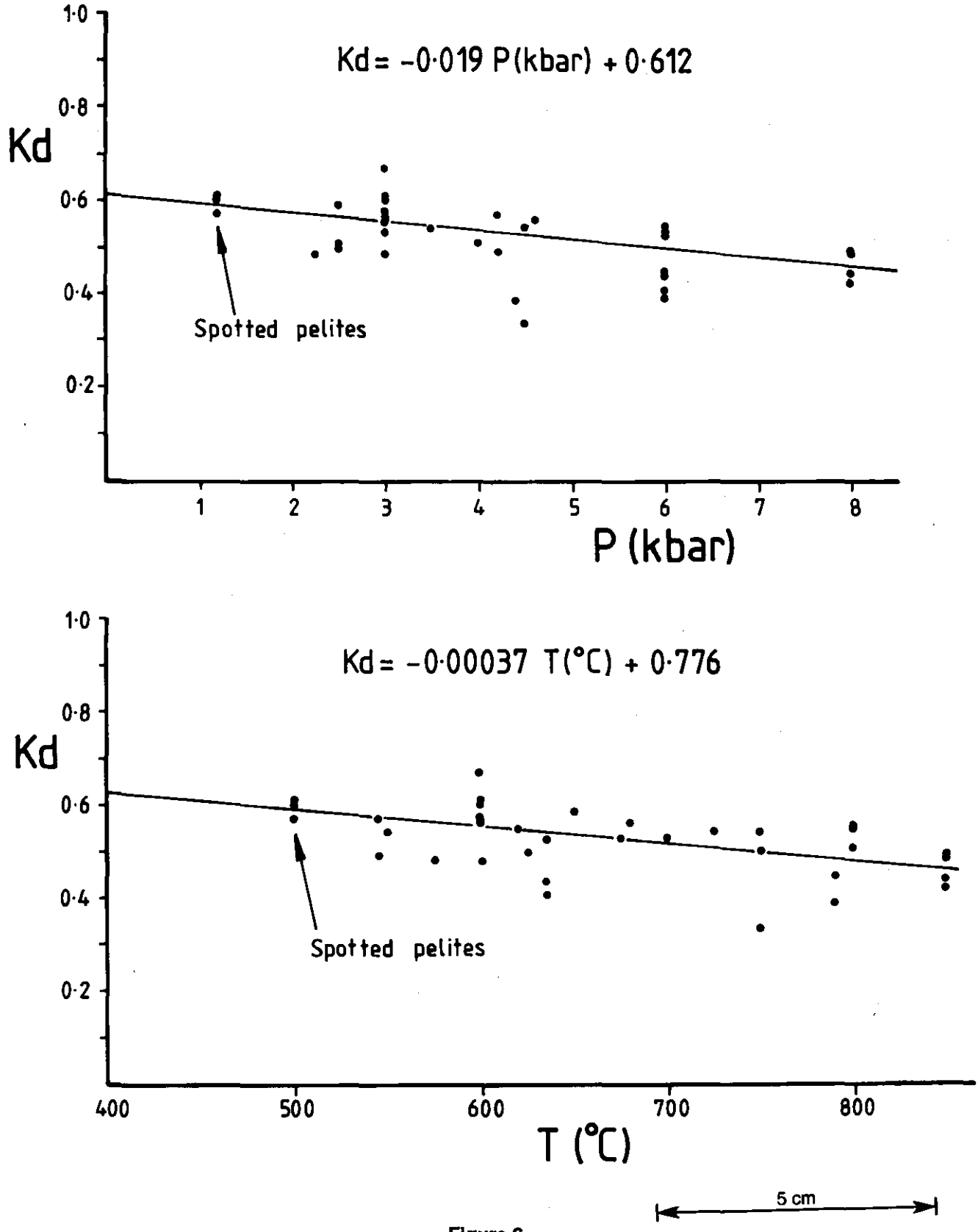

Figure 6

Fe-Mg exchange Kd for coexisting cordierite-biotite pairs from the literature are plotted against temperature and pressure estimates of formation by the same authors. Lines of "best fit" have not been statistically regressed but approximated by sight.